CrossMark

Effect of alkaline earth metal oxides on the dielectric, structural and physico-chemical properties of lithium–zinc–lead-borates

Reham M. M. Morsi[1] · Safeya Ibrahim[2] · Sherief Abo-Naf[2] · Morsi M. Morsi[2]

Abstract We report changes in the properties of lithium-zinc-lead-borate glass (mol%: $5Li_2O \cdot 10ZnO \cdot 60PbO \cdot 25B_2O_3$) brought by substituting alkaline earth metal oxides for part of its Li_2O content. These properties include density, optical basicity, molecular structure, conductivity, dielectric properties and chemical durability. The glasses were prepared by the melting quenching technique. The effect of substituting 2 mol% Li_2O by equivalent moles of MgO, CaO, SrO or BaO on the above mentioned properties is reported. The results showed that an increase in the density and the optical basicity is noticed for samples with substituted oxides in the order MgO, CaO, SrO or BaO. The FTIR also revealed that the BO_3 units with NBOs of the glasses increase with such substitution. The chemical durability was increased for glass with substituted MgO, while it decreased for those with substituted CaO, SrO or BaO. The conductivities of the base glass sample and that substituted with MgO are found to be mainly ionic while they are mainly electronic for those substituted with CaO, SrO or BaO. The dielectric permittivity revealed a value of 11.72 for the base un-substituted glass which increased to 394.02 at room temperature for glass substituted with BaO. The substituted samples with alkaline earth metal oxides produced glassy materials of high dielectric permittivity (ε') that could present good candidate for energy storage in electronic devices.

✉ Morsi M. Morsi
morsimmorsi@yahoo.com

1 Physical Chemistry Department, National Research Centre, 33 E l Bohoth st, Dokki, Cairo 12622, Egypt

2 Glass Research Department, National Research Centre, 33 E l Bohoth st, Dokki, Cairo 12622, Egypt

1 Introduction

Glassy materials containing heavy metal oxides particularly borate rich one have got special interest due to their possible applications as lamp phosphors and other photonic devices [1, 2]. Heavy metal oxide glasses also find applications in the field of optical fibers, optoelectronic devices; radiation shields, surgical lasers and their glass ceramic counterparts have wide range of applications [3]. Alkaline earth oxides improve glass forming capability while heavy metal oxides give rise to good optical properties such as second harmonic generation. [4].

Boric acid forms stable glasses with alkaline earth oxides (R = MgO, CaO, SrO, BaO) and heavy metal oxides (MO = ZnO, PbO, TeO_2, Bi_2O_3). The alkaline earth borate glasses containing heavy metal oxides show good solubility of rare-earth ions [4].

It is well known [5–7] that lead oxide (PbO) is unique in its influence on the glass structure and is widely used in glasses because it enhances the resistance against devitrification, improves the chemical durability and lowers the melting temperature. Lead oxide is considered as a nonconventional glass former, since it can act as a glass former or as a glass modifier. The role is determined by its concentration and by the type of bond between lead and oxygen [8]. Covalent bonding is associated with a network forming behavior, whilst an ionic bonding is related to glass modifier properties [9]. At high concentrations, PbO acts as a glass former [10], whilst at low concentrations it acts as a glass modifier [8]. Glasses with large amounts of PbO have been used widely in various commercial devices [11]. These glasses exhibit low glass transition temperatures (T_g) and high refractive indices [12].

The B_2O_3–PbO glasses have the desired characteristics against irradiation since the naturally occurring stable

boron isotope is a good absorber of thermal neutrons [13] and lead is known as a shielding material of γ-rays [14]. Lead borate glasses are already being used in enamels, photonics, and optoelectronic applications [8, 9]. A variety of anionic borate units such as penta-, tri-, tetra-, di-, pyro-, ortho-borate besides structural entities like boroxol ring have been identified in glasses containing B_2O_3 and PbO [15]. The concentration of these borate units in the glass structure is given by the nature and concentration of modifier oxide [16]. One reason for the interest in lead borate glasses is that binary borate glasses serve as model systems for structural analysis using tools such as NMR, FTIR, and Raman spectroscopy. A second reason is the technological potential of these glasses. The $PbO–B_2O_3$ system is one of the few binary borate systems which have actual and potential industrial applications. One of the main advantages of $PbO–B_2O_3$ glasses that sets them apart from other binary borate glasses are their relatively high chemical durability [17]. Lead borate and other low melting glasses are used in enamels, solders and seals applications [8, 18, 19].

Raman studies on some ternary lead borate glasses suggest that PbO may get incorporated into the network in four coordinated positions since the boron atoms in these glasses are both three (BO_3) and four coordinated (BO_4) [5]. The glass structure of lead oxide glasses is especially interesting, since up to 70 mol% of lead oxide can be incorporated in the glass network of ternary glasses. Usually, heavy metal oxide glasses contain 50–78 wt% of heavy metals, such as lead oxide [20].

When Boric acid is mixed with glass modifiers, such as Li_2CO_3 or other alkali oxides, its internal structure is rearranged due to the formation of non-bridging oxygens [20, 21]. A variety of metal oxides like MgO, CaO, SrO, BaO, ZnO, NiO, MnO, Al_2O_3, TiO_2, Ga_2O_3, etc., have been added and were found to be good stabilizers of borate glasses [22].

Glasses containing large amounts of Zinc oxide (ZnO) have low melting temperatures [23], which can be used for decoration as crystalline, crackle, opaque glasses with transparent spots and other decorative glasses [24]. The co-ordination state of Zn^{2+} ions in oxide glasses strongly suggests that ZnO_4 polyhedral plays an important role in forming glass network. Zn^{2+} ions will improve mechanical properties and chemical resistivity through the formation of tetrahedral co-ordination [23]. ZnO is considered as an important component for the preparation of multi-component oxide glasses with high thermal resistance against crystallization [25].

Borate glasses attracted the interest as a result of the fast ionic conductive properties exhibited by some of them, and the attractive possibilities they offer for energy storage applications [26]. Because in many applications glass must serve as an electrical insulator or semiconductor, so its electrical conductivity is important [27]. The present investigation is intended to report the influence of partial substitution of Li_2O by the modifier ions MgO, CaO, SrO or BaO on the electrical, dielectric properties and the internal molecular structure of lithium–zinc–lead-borate glasses. Their effects on the chemical durability, density and some physical parameters of the materials will be given.

2 Experimental methods

2.1 Glass samples preparation

Glasses of the compositions (mol%) $(5Li_2O - x)\cdot 10ZnO\cdot60PbO\cdot25B_2O_3$, x = 2MgO, 2CaO, 2SrO or 2BaO, were prepared using the melt-quench technique. The nominal compositions of the studied glasses are given in Table 1. Analar grade starting materials $MgCO_3$, $CaCO_3$, $SrCO_3$, $BaCO_3$, Li_2CO_3, ZnO, Pb_3O_4 and H_3BO_3 were used in the preparation of the glass batches. The intended materials were carefully weighed and thoroughly mixed in order to obtain a homogeneous mixture. The Weighed batches were melted in platinum crucibles at 1200 °C for 2 h. The melts were rotated at intervals of 30 min apart to ensure homogeneity of the melts. The melts were quenched in air on preheated stainless-steel molds of 1 × 1 × 3 cm dimensions (maintained at 100 °C). Then just after sitting, the solid glasses were directly transferred, to an annealing furnace at 450 °C to avoid the mechanical strain developed during the quenching process. The furnace was then switched off to cool to room temperature. The prepared samples were immediately transferred to a muffle furnace at 450 °C for annealing for 30 min which is then switched off to cool to room temperature. The obtained glass samples were transparent and yellow in color. The samples were checked by XRD and their amorphous nature is confirmed as shown in Fig. 1.

Table 1 Nominal chemical compositions (mol%) of the glasses studied

Glass no.	B_2O_3	PbO	ZnO	Li_2O	RO
G_0	25	60	10	5	–
G_{Mg}	25	60	10	3	2MgO
G_{Ca}	25	60	10	3	2CaO
G_{Sr}	25	60	10	3	2SrO
G_{Ba}	25	60	10	3	2BaO

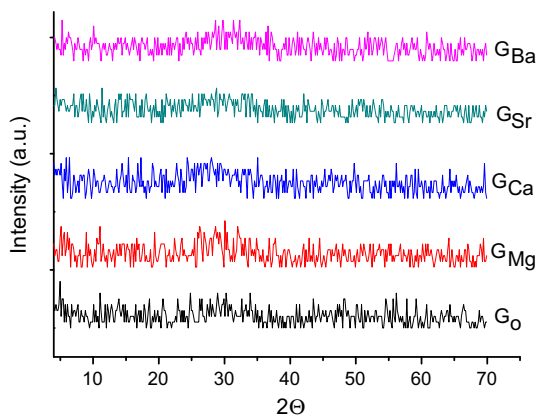**Fig. 1** XRD patterns of the samples studied

2.2 Density measurement

The density of each glass sample (ρ) was determined to an accuracy of ±0.001 by the Archimedes method using xylene as an inert immersion liquid. The density (ρ) was calculated by the relation;

$$\rho = \frac{W_a}{(W_a - W_b)} \times \rho_x,$$

where W_a is the weight of the glass sample in air, W_b is the weight of the glass sample immersed in xylene of density $\rho_x = 0.865$ gm cm^{-3}.

2.3 The optical basicity

The optical basicity Λ of a glass composed of mixed oxides can be calculated by the relation [28]:

$$\Lambda = \sum X_n \Lambda_n$$

where X_n is the equivalent fraction based on the amount of oxygen of each oxide contributes to the overall glass stoichiometry and Λ_n is the single oxides optical basicity. The optical basicity values of individual oxides are taken from the literature [29, 30] and are given by $\Lambda(B_2O_3) = 0.425$, $\Lambda(Li_2O) = 0.81$, $\Lambda(MgO) = 0.78$, $\Lambda(CaO) = 1.0$, $\Lambda(SrO) = 1.1$, $\Lambda(BaO) = 1.2$, $\Lambda(ZnO) = 0.95$ and $\Lambda(PbO) = 1.18$.

2.4 Chemical durability

The grain method carried out by several authors [31, 32] was followed to determine the chemical durability of the prepared glasses. Glass grains of 0.30–0.60 mm were immersed in distilled water (pH 7) for different times at 90 °C. 2 g of grains of each glass sample was placed in a sintered glass crucible G4 (Jena type) which was placed in a 250 ml polyethylene container containing 150 ml of the attacking solution (distilled water). The container was then situated in a water bath regulated at 90 °C. After different times, the container was removed from the bath and the sintered glass crucible was fitted on a suction pump and the whole solution was pumped through it. The sintered glass crucible was placed in air oven at 105 °C for 1 h. After cooling, the sintered glass crucible with its content was reweighed and the total loss in weight in the glass sample was calculated. The chemical durability of the glasses was evaluated from the measurement of the calculated dissolution rate (DR). The dissolution rate (g cm^{-1} min^{-1}) was calculated using the expression:

$$DR = (m_v - m_{rv})/A.t,$$

where m_v is the original weight of glass grains (g), m_{rv} is the weight after the dissolution test, A is the calculated area [33] of the glass grains (cm^2), and t is the time (min) of dissolution.

2.5 FTIR spectroscopy

For studying glass structure Fourier-transform infrared (FTIR) spectroscopy was performed using a Perkin–Elmer FT-IR spectrometer (model 1605) at wavelengths between 400 and 4000 cm^{-1}. Pellets of the powdered samples were prepared for FTIR measurements by mixing with spectroscopic grade dry KBr powder.

2.6 Electrical conductivity measurements

The electrical measurements were carried out on disc shaped samples using the technique described elsewhere [34]. The conductivity (σ_{ac}), dielectric permittivity (ε'), and the dissipation factor ($tan\delta$) of the prepared glass samples were measured using LRC Hi Tester (HIOKI, 3532-50). The frequency dependent measurements of capacitance, C, and dissipation factor, $tan\delta$, were obtained at temperature from 298 to 573 K. The dielectric permittivity (ε'), dielectric loss factor ($tan\delta$) and conductivity (σ) were determined from the following expression [35]:

$$\varepsilon' = C \cdot d/\varepsilon_o \cdot A,$$

where d is the thickness, A is the cross-sectional area, C is the capacitance of the sample, and ε_o is the free space permittivity. The temperature dependence of the ac conductivity, σ_{ac}, and dielectric permittivity, ε', are studied at frequency range from 0.1 Hz to 1 MHz at temperature range from 298 to 573 K. The ac conductivity, σ_{ac}, is calculated using the relation [36]:

$$\sigma = \omega\varepsilon_o\varepsilon' tan\delta,$$

where ω is the frequency of the input signal, $tan\delta$ is the dissipation factor or loss factor obtained from the

impedance analyzer. The measured total conductivity in terms of frequency is generally expressed as [36]:

$$\sigma_{Total} = \sigma_{dc} + \sigma_{ac} = \sigma_{dc} + A\omega^s,$$

where σ_{dc} is the frequency-independent component, A is a temperature dependent constant, S is the frequency exponent and ($\sigma_{ac} = A\omega^s$) represents ac or dissipative contribution to the total conductivity [37].

3 Results and discussion

3.1 Density

Table 2 depicts that the experimental density of the base glass G_0 (5.522 g cm^{-3}) increases to 5.567, 5.707, 5.899 or 5.982 as the alkaline earth metal oxides are substituted for 2 mol% Li$_2$O in the order MgO, CaO, SrO or BaO, respectively. The increase in the density can be attributed to the increase of the molecular mass of the substituted alkaline earth metal oxides. The increased density may also produce as a result of packing of the internal structure brought by the high efficient charges of the divalent cations.

3.2 Optical basicity

Table 2, lists the calculated theoretical optical basicity (Λ) for the glasses studied. The optical basicity (Λ) can be used to classify the covalent/ionic character of the glasses; it is higher for ionic bonding due to the fact that the charges around oxygen are localized around each element. Low value of Λ is typical of covalent bonding, where the oxygen shares its electrons with other elements, reducing its donor power [38]. Consequently, an increasing (Λ) indicates decreasing covalence of the glass network [39]. This decreasing covalence explains the finding (Table 2) that glass 1G$_0$ has the minimum (Λ) value (0.9398) which is found to increase to 0.9468 for glass G$_{Ba}$. The increasing ionic bonding accompanying the substitution of the divalent cations for the lithium ions is expected to cause more compaction for the glass structure. Consequently this effect may participate in the increased density of glasses G$_{Ca}$, G$_{Sr}$ and G$_{Ba}$.

According to Duffy et al. [40] the polarizability of oxygen ions is directly proportional to the optical basicity. The increase in the polarizability of oxygen ions is another indication that the concentration of NBOs increases [41]. In such a case it is expected that the glass G$_{Ba}$ should have more NBOs and its density would be lower than Glass G$_0$. The results of the density (Table 2) indicated that the rivers are found. This confirms that the increased density, as Li-ions are partially substituted by the divalent cations, is mainly due to the increase of their molecular weight while ionic bonding may play a minor effect.

3.3 Chemical durability

The dissolution rate of the glasses under the studied conditions versus ionic radius of alkaline earth cations are illustrated in Fig. 2. The results revealed that substituting 2 mol% of Li$_2$O by the alkaline earth oxide causes an increase in durability for glass G$_{Mg}$, and a decrease in the durability for glasses G$_{Ca}$, G$_{Sr}$ and G$_{Ba}$. When 2 mol% Li$_2$O was replaced by MgO the dissolution rate was decreased from 4.946 to 4.682 (10^{-4} g cm^{-2} min). Whereas replacing 2 mol% Li$_2$O by 2 mol% CaO, SrO or BaO the rate of dissolution was increased to 5.801, 5.381 or 5.945 (10^{-4} g cm^{-2} min), respectively.

When the Li$^+$ ions (0.76 Å) are replaced by the modifier ion Mg^{2+} (0.72 Å), this means replacing by a cation of higher effective charge. This condition favors more compaction of the glass structure that decreases its ability to be affected by the attacking medium. An attribution is given for the compactness of a lithium-containing phosphate glass when part of Li$_2$O was replaced by MgO as due to the large field strength of Mg^{2+} ions [42]. On the other hand replacing Li$^+$ ions successively by the ions of larger ionic radius viz., Ca^{2+} (1.00 Å), Sr^{2+} (1.18 Å) and Ba^{2+} (1.35 Å) in the glass network favors an open structure [43], consequently it becomes more liable to be chemically attacked and less durable.

3.4 Infrared transmission spectra

Infrared spectroscopy was used to obtain information concerning the internal structural units in the glasses studied. It is assumed that vibrations of characteristic

Table 2 Experimental density, optical basicity and dissolution rate of the glasses studied

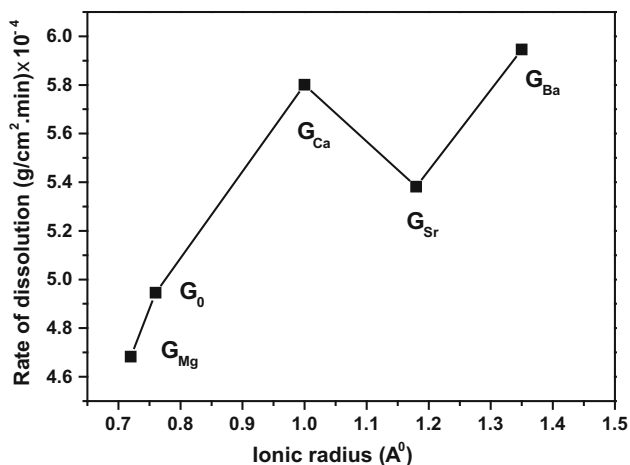| Glass code	Density (ρ) (gm cm^{-3})	Optical basicity (Λ)	Dissolution rate (g cm^{-1} min^{-1})
G$_0$	5.522	0.7678	4.946
G$_{Mg}$	5.567	0.7674	4.682
G$_{Ca}$	5.707	0.7703	5.801
G$_{Sr}$	5.899	0.7717	5.381
G$_{Ba}$	5.982	0.7730	5.945

Fig. 2 Dissolution rate of the un-substituted sample G_0 and after substituting 2 mol% of its Li_2O content with MgO, CaO, SrO or BaO (G_{Mg}, G_{Ca}, G_{Sr} and G_{Ba}, respectively) versus ionic radius of the alkali and alkaline earth cations

groups of atoms in the glass network are independent of vibration of other neighboring groups in the glass [44]. The infrared spectra of the glasses studies are shown in (Fig. 3). The IR spectra show various absorption bands which are characteristics of different vibrational modes. It can be seen that the absorption vibration modes are active in three IR spectral regions. The first region 400–800 cm^{-1} is assigned to bending vibrations of various borate segments and Pb–O bonds [9] as well as borate rings deformation [45]. The second region, 800–1100 cm^{-1} is assigned to stretching vibrations of BO_4 units in various structural groups [46].The third region 1100–1500 cm^{-1} is generally
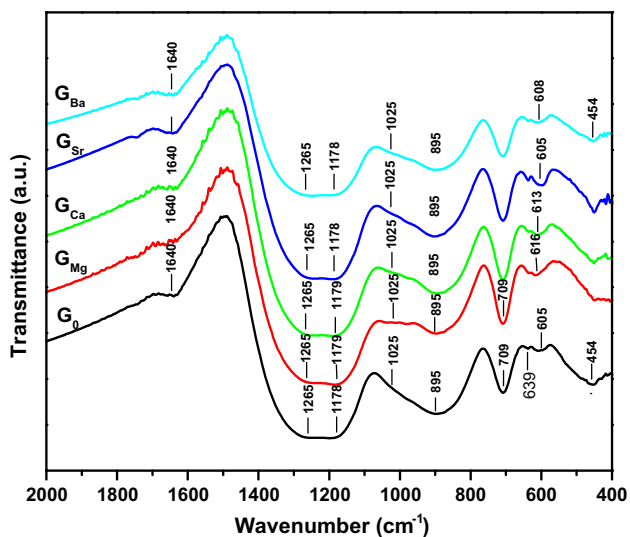

Fig. 3 FTIR spectra for the base glass with 5 mol% Li_2O and for the glasses with 2 mol% of Li_2O substituted by MgO, CaO, SrO or BaO (G_{Mg}, G_{Ca}, G_{Sr} and G_{Ba}, respectively)

ascribed to the B–O stretching and $B–O^-$ stretching vibrations of BO_3 and BO_2O^- units respectively [46–48]. Table 3 lists the assignment of the observed infrared absorption bands in the spectra of the glasses studied.

In the first region, the band at about 454 cm^{-1} observed in all spectra of the glasses is assigned to angles modification of the B–O–B linkages [49, 50]. The absorption band at this frequency is also reported to be associated with vibrations of PbO_4 structural units [16]. The intensity band at 605 cm^{-1} for glass G_0 increases and appears at 616, 613, 605 and 608 cm^{-1} on the substitution of 2 mol% Li_2O by MgO, CaO, SrO or BaO, respectively. A weak band is observed at 639 cm^{-1} for all glasses can be attributed to a bending mode of the Pb–O–B links [5]. A sharp band at 709 cm^{-1} is observed in all glasses due to B–O–B bending vibrations of various borate segments [45]. The sharpness of this band has been attributed to presence small proportions of pyroborate units in the glass structure [5].

In the second region, a broad absorption band is observed in all spectra with a peak at 895 cm^{-1} and a shoulder at 1025 cm^{-1} due to B–O vibrations in BO_4. [50–52]. The intensity of the shoulder at 1025 cm^{-1} is decreased dramatically in the spectra of the substituted glasses.

In the third region, the absorption bands at 1178 and 1265 cm^{-1} can be assigned to BO_3 vibrations in metaborate and ortho-borate groups, respectively [5, 9, 46, 53].

The absorption peak observed at 1640 cm^{-1} for all spectra is attributed to H–O–H bending mode [54]. The decreased intensity of this absorption band for glass G_{Mg} which is more chemically durable than glass G_0 (Table 2) confirm the compactness of structure of glass G_{Mg}. On the contrary, the still persisting intensity of this band for glasses G_{Ca}, G_{Sr} and G_{Ba}, indicates their open structure nature, which is consistent with their lower durability (Fig. 2).

It is worthy noticing (Fig. 3) that, the overall absorptions of BO_4 bands (800–1100 cm^{-1}) decrease relative to BO_3 absorption bands (1100–1500 cm^{-1}) on substitution 2 % Li_2O with MgO, CaO, SrO or BaO. The increase of the BO_3 absorption bands reveals the increase of structural units with NBOs. This is due to the modifying action of the modifiers, where the bigger cations are in favor of the formation of NBOs in alkali borate glasses [55].

3.5 Electrical and dielectric properties

Figure 4 represents the frequency dependence of σ_{ac} for sample G_0 (as a representative sample) at various temperatures. Plots of log σ_{ac} versus log f indicate that σ_{ac} increases with frequency and follows the power law, $\sigma_{ac} = A \omega^s$, in the studied frequency range. The slopes of the curves (d log σ_{ac}/d log f) for sample G_0 represent the

Table 3 Assignment of measured Infrared band positions for the investigated glasses

Band positions (cm^{-1})	Assignments	References
454	Bending vibrations of O–B–O bond, overlapping with Pb–O bond vibrations	[16]
605	Bending vibrations of O–B–O bond	[16]
639	Can be attributed to a bending mode of the Pb–O–B links	[5]
709	Bending vibrations of B–O–B linkage in the borate network	[45]
895	Stretching modes B–O in BO_4 groups	[51]
1025	Stretching vibrations of B–O in BO_4 units from tri- tetra- and penta-borate groups.	[50, 52]
1178	Stretching vibrations of bridging oxygens in trigonal borons	[53]
1265	Asymmetric stretching vibrations of BO_3 units and BO_2O^- in metaborate and ortho-borate groups, or combination of the latter vibration and $[PbO_{4/2}]^{2-}$ vibration.	[9, 46, 5]
1640	Bending mode of H–O–H	[54]
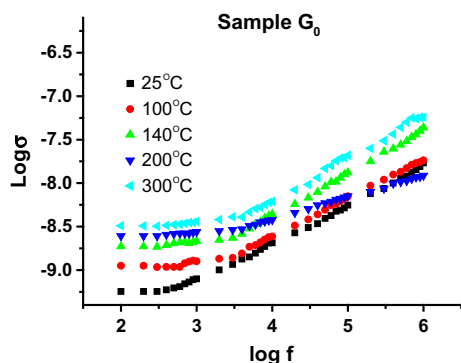
Fig. 4 The frequency dependence of σ_{ac} for the un-substituted sample G_0 at various temperatures

exponent S, where $0 < s < 1$. The direct current (dc) conductivities of the samples are generated from the plateau regions by extrapolating to zero frequency [56]. The variation of log σ_{ac} with (log f) for the studied glass samples G_0, G_{Mg}, G_{Ca}, G_{Sr} and G_{Ba} at room temperature was drawn for comparison (Fig. 5). It is clear from this
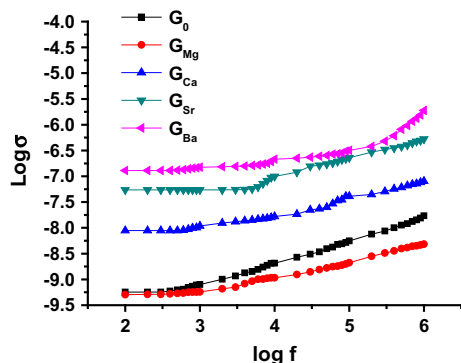

Fig. 5 The frequency dependence of σ_{ac} for the substituted samples G_0, G_{Mg}, G_{Ca}, G_{Sr} and G_{Ba} at room temperature

figure that the power law is also followed for all glass compositions. The values of (s) are calculated for all glass compositions at different temperatures and listed in Table 4.

Figure 6 shows a plot for the values of the frequency exponent (s) at different temperatures for the glass samples (G_0, G_{Mg}, G_{Ca}, G_{Sr} and G_{Ba}). It can be noticed that at room temperature sample G_{Ba} showed the maximum value (0.95) for the frequency exponent (s) which is decreased to a value of (0.3) for sample G_{Mg}. Generally, it is known that (s) represents a measure of the degree of interaction of the charge carriers with the environment [57]. To precise the predominant conduction mechanism under AC field for the studied samples, one can suggest the appropriate model in the light of the different theoretical models. These models correlate the conduction mechanisms of AC conductivity with the frequency exponent (s) behavior as follows:

1. The exponent (s) is almost equal to 0.8 and slightly increases with temperature or independent of temperature, in case of the quantum mechanical tunneling (QMT) model, [58].

2. The exponent (s) increases with increasing temperature in case of the small polaron SP model [59, 60],

3. The exponent (s) depends on both frequency and temperature and drops with rising temperature to a minimum value then increases, as temperature rises in the case of overlapping-large polaron tunneling (OLPT) model [61].

4. The values of the frequency exponent (s) are decreased with increasing temperature in the case of the correlated barrier hopping (CBH) model [62].

From Fig. 6, it is clear that the frequency exponent (s) for samples (G_0, G_{Mg}, G_{Ca} and G_{Sr}) exhibits two distinct regions: Region (I) from room temperature up to 200 °C, in which a slight decrease in (s) with increasing temperature

Table 4 Calculated values of dc conductivity (σ_{dc}) at RT, dc activation energy ($E_{a(dc)}$), permittivity (ε') at 100 Hz and 1 MHz in the temperature range (298–573 K) and frequency exponent s for, all studied samples

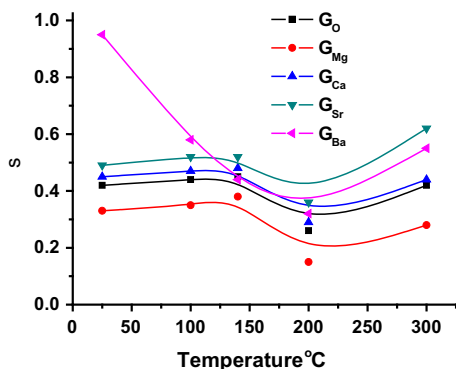| Glass no.	ε' (100 Hz)		ε' (1 MHz)		S (at RT)	σ_{dc} (S cm^{-1})	$E_{a(dc)}$ (eV)
	25 °C	300 °C	25 °C	300 °C			
G_0	11.72	141.24	5.38	10.21	0.42	5.04×10^{-10}	0.55
G_{Mg}	102.97	659.23	6.15	15.83	0.33	5.67×10^{-10}	1.70
G_{Ca}	132.53	531.19	14.00	20.68	0.45	8.89×10^{-9}	0.20
G_{Sr}	294.41	623.98	16.01	21.30	0.49	5.44×10^{-8}	0.15
G_{Ba}	394.02	782.68	32.45	35.94	0.95	1.29×10^{-7}	0.13

Fig. 6 The temperature dependence of frequency exponent (s) for the substituted glass samples G_0, G_{Mg}, G_{Ca}, G_{Sr} and G_{Ba}

Fig. 7 Variation of log conductivity versus 10^3/T (K^{-1}) for the un-substituted glass (G_0) and after substituting 2 mol% of its Li$_2$O by MgO, CaO, SrO or BaO (G_{Mg}, G_{Ca}, G_{Sr} and G_{Ba}, respectively)

according to barrier hopping (CBH) is shown. This indicates that the thermally activated behavior of electron transfer over the barrier between two sites having their own columbic potential wells is valid [63]. Region II (above 200 °C) in which an increase in (s) on increasing temperature according to small polaron (SP) tunneling is noticed. This indicates that the activated behavior of polaron is independent of intersite separation [63]. However, for sample G_{Ba} on increasing temperature the exponent (s) decreases from 0.95 at room temperature to a minimum value, and then it increases in a manner similar to small polaron. According to some authors [62, 64] this means that the exponent (s) fits OLPT model for this glass sample.

Figure 7 shows the variation of log conductivity versus 10^3/T (K^{-1}). The DC activation energies are calculated for all the samples using the Arrhenius relation:

$$\sigma = \sigma_0 exp(-E/KT),$$

where K is Boltzmann constant, E is activation energy and σ_0 is the pre exponential factor. The activation energies are listed in Table 4 from which it can be noticed that the base glass showed activation energy of 0.55 eV while glass G_{Mg} showed the highest activation energy (1.70 eV). For glass samples G_{Ca}, G_{Sr} or G_{Ba} the activation energy decreases to 0.20, 0.15 or 0.13 (eV), respectively. The conductivity values (Table 4) reveal that, the conductivity increases for the substituted glasses which attained the highest value
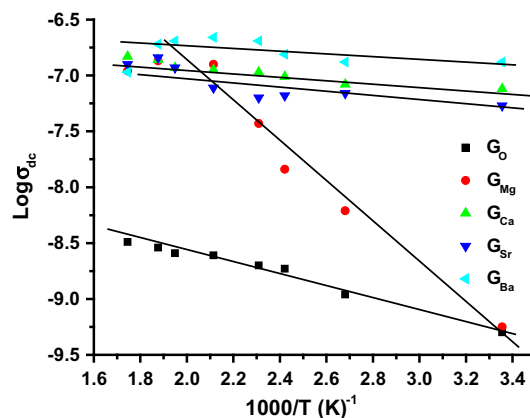
(1.29×10^{-7} S.cm^{-1}) for glass G_{Ba}. These results are consistent with the recorded (s) value for glass G_{Ba}, as it is reported that the more conducting glasses have higher (s) values [65].

For the base glass G_0 Li$^+$ ions seem to be the main carriers. On replacing 2 mol% of alkaline earth oxide for 2 mol% Li$_2$O, there should be 2 mol of bivalent ions are introduced at the expense of 4 mol Li$^+$ ions. The larger reduction in Li$^+$ concentration due to the substitutions with alkali-earth metal ions is expected to decrease the ionic carriers, consequently leading to a reduction in ionic conductivity. However, for glass G_{Mg}, partial replacing of Mg-ions for Li$^+$ causes an increase in conductivity, despite its higher activation energy. The ionic conductivity contribution by Mg-ions for glass G_{Mg} explains its high activation energy value, while the electronic conductivity contribution seems to increase the observed conductivity. The high electrical field strength of Mg^{2+} is the cause of the high activation energy of this glass (1.70 eV). From IR results (Fig. 3) the partial replacement of MgO for Li$_2$O causes an increase in the BO$_3$ units which provide the glass structure with NBOs. The latter may explain the increase of the expected contribution of the electronic conduction of glass G_{Mg}. From the above findings it can be concluded that, the conduction is mainly ionic in glasses G_0 and G_{Mg}.

The higher conduction of glasses G_{Ca}, G_{Sr} or G_{Ba} than glass G_0 or G_{Mg}, which is accompanied with their low activation energy, can be attributed to the prevalence of electronic carriers. The relatively large ionic radius of Ca, Sr or Ba ions (1.0, 1.18, 1.35 Å, respectively) and their small electrical field strength, cause the glass structure to be more opened. Taking into consideration that BO_3 units are prevailing in these glasses, the formed NBOs provide the electronic carriers which move easily in these open glass structure. The latter explains the lower activation energies of these glasses (0.20–0.13 eV) which suggest that the conduction in glasses G_{Ca}, G_{Sr} or G_{Ba} is mainly electronic.

Figure 8 shows the frequency dependence of the dielectric permittivity (ε') measured at different temperatures for sample G_0 (as an example). It can be observed that sample G_0 exhibits high dielectric permittivity at low frequencies which decreases with increasing the frequency. The decrease in dielectric permittivity with increasing frequency can be attributed to the contribution of the multi-component of polarization [66]. These polarizations are considered as, electronic, ionic, dipolar or orientation and space charge [67]. The first (valance electrons relative nucleus polarization) occurs at frequencies up to 10^{16} Hz. The second (ionic polarization) occurs due to the displacement of negative and positive ions with respect to each other. The maximum frequency of ionic polarization is 10^{13} Hz. The third (dipole polarization) occurs as a result of the presence of molecules with permanent electric dipole moments that can change orientation into direction of the applied electric filed. Dipole polarization occurs at frequencies up at about 10^{10} Hz. Finally, space-charge polarization occurs due to impedance mobile charge by interface. Space-charge polarization typically occurs at frequencies between 1 and 10^3 Hz. The total polarization of dielectric material can be represented by the sum of thes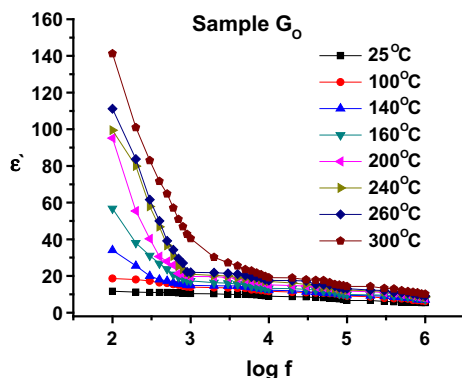e four polarizations [67, 68]. In other words, as the frequency increases the dipoles will no longer be able to rotate sufficiently, so that their oscillation will begin to lag behind those of the field. Hence dielectric permittivity at high frequencies is decreased and approaches nearly a limit value [69, 70].

The dependence of the dielectric permittivity (ε') on temperature was studied for the investigated glass samples at 1 MHz as shown in Fig. 9. As observed from this figure, the dielectric permittivity increases with increasing temperature. It can also be seen that, substituting the alkaline earth oxides for 2 mol% Li_2O increases the dielectric permittivity of the present glasses in the order MgO < CaO < SrO < BaO. These conditions may lead to an increase of the ion motion, consequently increases the dielectric permittivity [71].

Figure 10 shows the variation of dielectric permittivity with the activation energy for the base glass and after substituting alkaline earth oxide for 2 mol% Li_2O. For the glasses G_{Mg}, G_{Ca}, G_{Sr} and G_{Ba} it can be noticed that the ε' tends to vary inversely with the activation energy. At room temperature glass G_{Mg} revealed activation energy of 1.70 (eV) and ε' of 103 at 100 Hz while glasses G_{Ca}, G_{Sr} and G_{Ba} revealed activation energies in the range of 0.13–0.17 (eV) and ε' in the range of 132–394 at 100 Hz. This behavior is also valid for the data obtained at higher frequencies (1 MHz).

4 Conclusions

Replacing 2 mol% of the lithium oxide of the lithium–zinc–lead borate glass by equivalent moles of MgO, CaO, SrO or BaO increases the experimental densities and optical basicity of the glasses. The increase of the optical basicity indicates an increasing polarizability.

Substituting 2 mol% of Li_2O by the alkaline earth oxide causes an increase in durability for glass substituted with
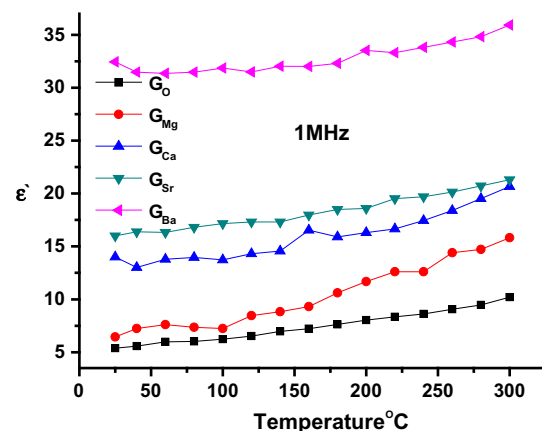

Fig. 8 Frequency dependence of the dielectric permittivity (ε') for the un-substituted sample G_0 measured at different temperatures

Fig. 9 Temperature dependence of the dielectric permittivity (ε') measured at 1 MHz and room temperature for the glasses studied
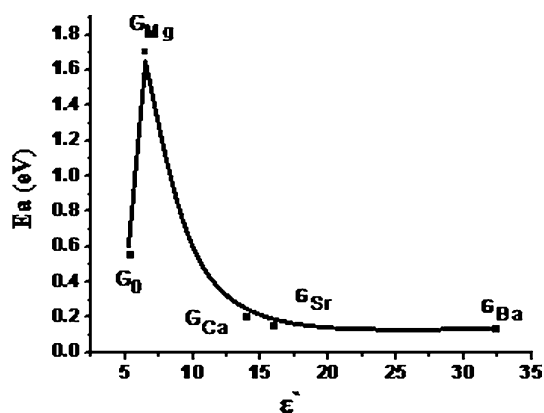
Fig. 10 Variation of activation energy with the permittivity (ε') measured at 1 MHz for the Li–zinc–lead borate glass samples before (G_0) and after substituting 2 mol% of its Li_2O by MgO, CaO, SrO or BaO (G_{Mg}, G_{Ca}, G_{Sr} and G_{Ba}, respectively)

MgO, and a decrease in the durability for glasses substituted with CaO, SrO and BaO.

When the Li^+ ions are replaced by modifier ion of Mg^{2+} which is replaced successively by the ions of larger radii viz., Ca^{2+}, Sr^{2+} and Ba^{2+}, causes a decrease in BO_4 and increase in the BO_3 structural units which are accompanied with increase in the NBOs.

The dielectric permittivity (ε') of the lithium–zinc–lead borate sample is found to be temperature and composition dependent. At room temperature (and 0.1 kHz) it attains a value of 11.72 which increases to 102.97, 132.53, 294.41 or 394.02 on substitution of 2 mol% Li_2O by MgO, CaO, SrO or BaO, respectively. At high temperature (300 °C) and 0.1 kHz the same behavior is valid, yet with much higher dielectric permittivity values. These substitutions produce materials with high dielectric permittivity (ε') that could present good candidate for energy storage in electronic devices.

The substitution of 2 mol% Li_2O by MgO, CaO, SrO and BaO leads to frequency exponent (s) values between 0.15 and 0.95. The conduction mechanism for base and the substituted glass samples occurs according to CBH and SP models, yet for sample substituted with BaO the conduction occurs according to (OLPT) model. The conduction is mainly ionic in the base lithium-zinc-lead-borate glass and the substituted MgO for 2 mol% Li_2O, while it is mainly electronic for glasses with the substituted CaO, SrO and BaO for 2 mol% Li_2O.

References

1. G.D. Khattak, N. Tabet, Phys. Rev. B **72**, 104203 (2005)
2. S. Murugavel, B. Roling, Phys. Rev. B **76**, 180202 (2007)
3. Ch. Rajasree, K. Rao, J. Non-Cryst. Solids **357**, 836 (2011)
4. S.L.S. Rao, G. Ramadevudu, Md Shareefuddin, A. Hameed, M.N. Chary, M.L. Rao, Int. J. Eng. Sci. Technol. **4**, 25 (2012)
5. M. Ganguli, K.J. Rao, J. Solid State Chem. **145**, 65 (1999)
6. P.J. Bray, M. Leventhal, H.O. Hooper, Phys. Chem. Glasses **4**, 47 (1963)
7. B.N. Meera, A.K. Sood, N. Chandrabhas, J. Non-Cryst. Solids **126**, 224 (1990)
8. Y.B. Saddeek, J. Alloys Compd. **467**, 14 (2009)
9. R.C. Lucacel, I. Ardelean, J. Non-Cryst. Solids **353**, 2020 (2007)
10. Y. Cheng, H. Xiao, W. Guo, Ceram. Int. **33**, 1341 (2007)
11. T. Inoue, T. Honma, V. Dimitrov, T. Komatsu, J. Solid State Chem. **183**, 3078 (2010)
12. V. Dimitrov, S. Sakka, J. Appl. Phys. **79**, 1736 (1996)
13. V.F. Sears, Neutrons News **3**, 26 (1992)
14. H. Ushida, Y. Iwadate, T. Hattori, J. Alloys Compd. **377**, 167 (2004)
15. G.D. Chryssikos, E.I. Kamitsos, M.A. Karakassides, Phys. Chem. Glasses **31**, 109 (1990)
16. R.C. Lucacel, C. Marcus, V. Timar, I. Ardelean, Solid State Sci. **9**, 850 (2007)
17. C. Erdogan, M. Bengisu, S.A. Erenturk, J. Nuclear Mater. **445**, 154 (2014)
18. S. Rada, P. Pascuta, M. Culea, V. Maties, M. Rada, M. Barlea, E. Culea, J. Mol. Struct. **924–926**, 89 (2009)
19. N.M. Bobkova, Glass Ceram. **66**, 206 (2009)
20. J. Coelho, C. Freire, N.S. Hussain, Spectrochim. Acta, Part A **86**, 392 (2012)
21. Y.B. Saddeek, L.A.E. Latif, Phys. B **348**, 475–484 (2004)
22. M.S. Reddy, G.N. Raju, G. Nagarjuna, N. Veeraiah, J. Alloys Compd. **438**, 41 (2007)
23. A. Thulasiramudu, S. Buddhudu, J. Quant. Spectrosc. Radiat. Transf. **97**, 181 (2006)
24. S. Stefanov, Glass Tech. **41**, 193 (2000)
25. K. Aida, T. Komatsu, V. Dimitrov, Phys. Chem. Glasses **42**, 103 (2001)
26. H.L. Tuller, P.K. Moon, Mater. Sci. Eng. B **1**, 171 (1988)
27. N.K. Sanjay, A. Agarwal, J. Alloys Compd. **487**, 52 (2009)
28. J.A. Duffy, M.D. Ingram, in *Optical Properties of Glass*, ed. by D. Uhlman, N. Kreidl, Am. Ceram. Soc. Westervill (1991)
29. V. Dimitrov, T. Komatsu, J. Ceram. Soc. Jpn. **107**, 1012 (1999)
30. V. Dimitrov, T. Komatsu, J. Univ. Chem. Technol. Met. (Sofia) **45**, 219 (2010)
31. S. Ibrahim, M.M. Morsi, Mater. Chem. Phys. **138**, 628 (2013)
32. I. Szabo, G. Volksch, W. Holland, J. Non-Cryst. Solids **272**, 191 (2000)
33. P.B. Adams, M.E. Mordberg, H.V. Wolters, Glass Technol. **5**, 136 (1964)
34. R.M.M. Morsi, S. Ibrahim, M.M. Morsi, J. Mater. Sci.: Mater. Electron. **26**, 1419 (2015)
35. B. Kumar, T. Vijaya, M. Sankarappa, S. Kumar, P.J.P. Kumar, R. Sadashivaiah, R. Reddy, Phys. B **404**, 3487 (2006)
36. J.C. Dyre, J. Non-Cryst. Solids **135**, 219 (1991)
37. H. El Mkami, B. Deroide, R. Backov, J.V. Zanchetta, J. Phys. Chem. Solids **61**, 819 (2000)
38. E. Kamitsos, Y. Yiannopoulos, J. Duffy, J. Phys. Chem. B **106**, 8988 (2002)
39. S. Sanghi, S. Rani, A. Agarwal, V. Bhatnagar, Mater. Chem. Phys. **120**, 381 (2010)
40. J.A. Duffy, Phys. Chem. Glasses **30**, 1 (1989)
41. R.J.G.P.L. Higby, I.D. Aggarwal, E.J. Friebele, J. Non-Cryst. Solids **126**, 209 (1990)
42. R. Yang, Y. Wang, X. Hao, J. Zhan, S. Liu, J. Non-Cryst. Solids **357**, 2192 (2011)
43. A.I. Priven, Glass Phys. Chem. **26**, 541 (2000)
44. P. Pascuta, S. Rada, G. Borodi, M. Bosca, L. Popa, E. Culea, J. Mol. Struct. **924–926**, 214 (2009)

45. W.A. Pisarski, T. Goryczka, B. Wodecka-Dús, M. Płónska, J. Pisarska Mater. Sci. Eng. B **122**, 94 (2005)

46. E.I. Kamitsos, A.P. Patsis, M.A. Karakassides, G.D. Chryssikos, J. Non-Cryst. Solids **126**, 52 (1990)

47. B.K. Sudhakar, N.R.K. Chand, H.N.L. Prasanna, G.S. Rao, K.V. Rao, V. Dhand, J. Non-Cryst. Solids **356**, 2211 (2010)

48. B. Sumalatha, I. Omkaram, T.R. Rao, ChL Raju, Phys. B **411**, 99 (2013)

49. G.E. Walrafen, S.R. Samanta, P.N. Krishnan, J. Phys. Chem. **72**, 113 (1980)

50. I. Ardelean, C. Simona, R. Dorina, Phys. B **403**, 3682 (2008)

51. O. Cozar, I. Ardelean, I. Bratu, S. Simon, C. Craciun, L. David, C. Cefan, J. Mol. Struct. **563**, 421 (2001)

52. P. Pascuta, B. Gheorghe, C. Eugen, J. Non-Cryst. Solids **354**, 5475 (2008)

53. A.K. Hassan, L. Borjesson, L.M. Torell, J. Non-Cryst. Solids **172–174**, 154 (1994)

54. B. Karthikeyan, S. Mohan, Phys. B **334**, 298 (2003)

55. R.B. Rao, R.A. Gerhardt, Mater. Chem. Phys. **112**, 186 (2008)

56. I. Gustian, S.Ü. Çelik, A. Zainuddin, W. Suratno, A. Bozkurt, R.E. Siregar, J. Math. Fund. Sci. **46**, 50 (2014)

57. R. Vaish, K.B.R. Varma, Phys. Rev. B **42**, 1388 (1990)

58. ShA Mansour, I.S. Yahia, F. Yakuphanoglu, Dyes Pigments **87**, 144 (2010)

59. N.F. Mott, J. Non-Cryst. Solids **1**, 1 (1968)

60. M.H. Buraidah, L.P. Teo, S.R. Majid, A.K. Arof, Phys. B **404**, 1373 (2009)

61. J.T. Gudmundsson, H.G. Svavarsson, S. Gudjonsson, H.P. Gislason, Phys. B **340**, 324 (2003)

62. W. Jung, Phys. B **403**, 636 (2008)

63. R. Kumar, S.K. Arora, I.V. Shvets, N.E. Rajeevan, P.P. Pradyumnan, D.K. Shukla, J. Appl. Phys. **105**, 07D910 (2009)

64. E. Abd El-Wahabb, Acta Phys. Pol. A **108**, 985 (2005)

65. S. Mahadevan, A. Giridhar, K.J. Rao, J. Phys. C: Solid State Phys. **10**, 4499 (1977)

66. E.M.A. Hamzawy, R.M.M. Morsi, F.H. Margha, J. Mater. Sci.: Mater. Electron. **26**, 1252 (2015)

67. M.H. Suhail, I.M. Al-Essa, R.A. Ahmed, Int. J. Eng. Tech. Res. (IJETR) **2**, 379 (2014)

68. M.W. Barsoum, *"Fundamentals of Ceramics", (Series in Material Science and Engineering)* (McGraw-Hill, New York, 1977), p. 543

69. F. Carpi, D.D. Rossi, R. Kornbluh, R. Pelrine, P.S. Larsen (eds.), *Dielectric Elastomers as Electromechanical Transducers* (Elsevier, Hungary, 2008), p. 344

70. N.D. Sankır, E. Aydın, M. Sankır, Int. J. Electrochem. Sci. **9**, 3864 (2014)

71. A.G. Mostafaa, A.H. El-Dosokey, K.H. Idress, H.M. Goumaa, Int. J. Res. Eng. Sci. (IJRES) **2**, 58 (2014)